AIAA-99-4106

AN INTEGRATED VEHICLE MODELING ENVIRONMENT

Joseph J. Totah[*], Dr. David J. Kinney[*], John T. Kaneshige[†], and Shane Agabon[‡]
NASA Ames Research Center
Moffett Field, California

Abstract

This paper describes an Integrated Vehicle Modeling Environment for estimating aircraft geometric, inertial, and aerodynamic characteristics, and for interfacing with a high fidelity, workstation-based flight simulation architecture. The goals in developing this environment are to aid in the design of next generation intelligent flight control technologies, conduct research in advanced vehicle interface concepts for autonomous and semi-autonomous applications, and provide a value-added capability to the conceptual design and aircraft synthesis process. Results are presented for three aircraft by comparing estimates generated by the Integrated Vehicle Modeling Environment with known characteristics of each vehicle under consideration. The three aircraft are a mid-sized, twin-engine commercial transport concept, a modified F-15 with moveable canards attached to the airframe, and a small, single-engine, uninhabited aerial vehicle. Estimated physical properties and dynamic characteristics are correlated with those known for each aircraft over a large portion of the flight envelope of interest. The results show significant improvement in estimating vehicle aerodynamic characteristics using an improved vortex lattice code, and represent the completion of a critical step toward meeting the stated goals for developing this modeling environment.

Introduction

Next generation intelligent flight control technologies are being developed to exhibit higher levels of adaptability and autonomy than current state-of-the-art systems for the purpose of automatically compensating for a broader spectrum of damaged or malfunctioning aircraft, controlling remote or autonomous vehicles, and reducing costs associated with flight control law development. Advanced vehicle interface concepts are also being studied principally as an alternate approach for interacting with autonomous and semi-autonomous aircraft and associated data rich environments that might accompany their applications.

The Integrated Vehicle Modeling Environment described in this paper was developed so that a variety of different aircraft could be examined using these new technologies and concepts. The intent was to ensure applicability to many vehicle classes including commercial transports, high performance military aircraft, hypersonic vehicles, remotely piloted or uninhabited concepts, reusable launch vehicles, and autonomous planetary aircraft.

The work presented in this paper builds upon previous work by Totah and Kinney[1] by incorporating improvements in estimating aerodynamic stability and control characteristics, incorporating a high-fidelity, workstation-based flight simulation architecture, and integrating these technologies using a seamless, user-friendly graphical interface. This work was sponsored by the Intelligent Flight Control element of the Information Technology R&T Base Program managed at NASA Ames Research Center.

Integrated Vehicle Modeling Environment

The Integrated Vehicle Modeling Environment (IVME) is comprised of several different computer programs controlled by a graphical user interface written in the Java programming language. The programs are used to estimate aircraft geometric, aerodynamic, and inertial characteristics, reformat graphics and data, and train neural networks, the results of which are ultimately used in a high fidelity workstation-based simulation environment.

The programs comprising the IVME are shown in figure 1, where each block represents a different program and the lines connecting the blocks represent the transfer of data from one program to another in a sequential fashion. Programs are invoked by simply clicking on the block, thereby enabling user access. This section describes how the IVME is used to develop models for three different aircraft; namely a commercial transport, a fighter, and a small,

---

[*] Aerospace Engineer, Senior Member AIAA
[†] Computer Engineer, Member AIAA
[‡] Student Intern, Foothill Community College

uninhabited aerial vehicle (UAV). The next section describes the simu[illegible]nt and the flight control architectu[illegible]rcraft.

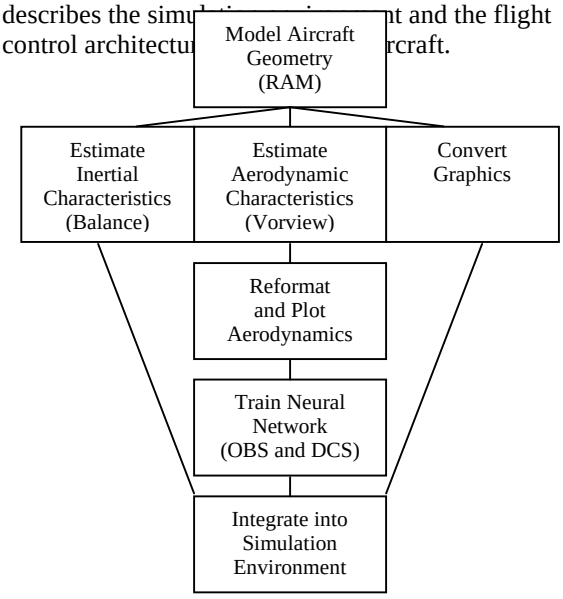

Figure 1. Integrated Vehicle Modeling Environment.

The first step in developing aircraft models using IVME is to create a computer image to match a scaled drawing of the vehicle as closely as possible. The program used to create a three-dimensional image of the aircraft is the Rapid Aircraft Modeler (RAM), developed internally at NASA Ames. Three completely different aircraft types were created using RAM; a twin-engine mid-sized commercial transport concept shown in figure 2, the F-15 Advanced Control Technologies for Integrated Vehicles (ACTIVE) aircraft shown in figure 3, and the LoFLYTE™ UAV shown in figure 4.

Figure 2. Commercial Transport RAM Model.

The commercial transport concept shown in figure 2 is based on a flight simulation developed by Lockheed Georgia Company in 1983 for the six degree-of-freedom Advanced Concepts Flight Simulator (ACFS) at NASA Ames[2]. The simulator has been used extensively for human factors research, and most recently to study propulsion-only control and flight director aids.

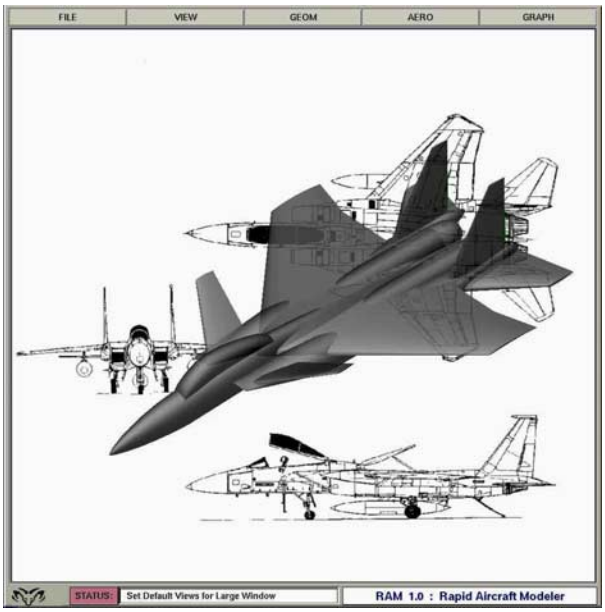

Figure 3. F-15 ACTIVE RAM Model.

The F-15 ACTIVE aircraft shown in figure 4 is currently in operation at NASA Dryden. It is not a conventional F-15 in that it has canards and thrust vectoring nozzles. The aircraft is configuration G of the US Air Force's Short takeoff and landing Maneuver Technology Demonstrator (S/MTD) program.[3]

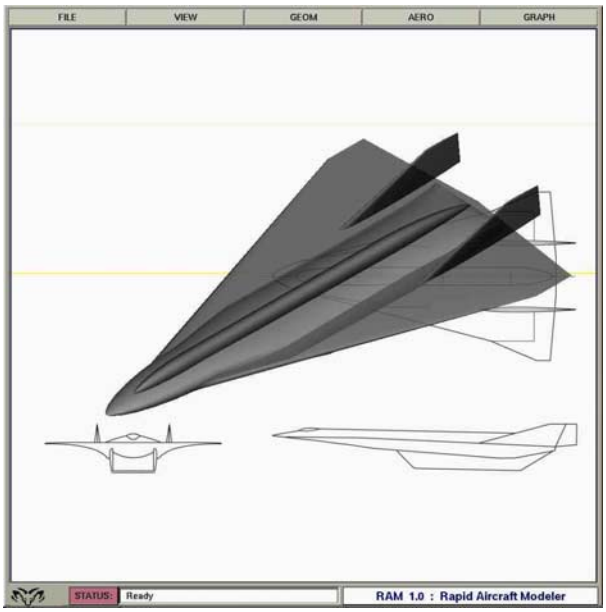

Figure 4. LoFLYTE™ RAM Model.

The LoFLYTE™ UAV shown in figure 5 was developed by Accurate Automation Corporation in cooperation with NASA Langley Research Center and the US Air Force Research Laboratory at Wright-Patterson Air Force Base. It is currently in operation to study adaptive and fault tolerant neural flight control technologies.

Once RAM models have been completed, they can be converted to the Open Inventor graphics format for Silicon Graphics workstations. This useful option allows aircraft models to be seamlessly imported into a graphical database that is driven by the simulation environment described in the next section.

After RAM models have been created, the program "Balance" is then used to estimate aircraft center-of-gravity (CG) and inertial characteristics. This program, also developed internally at NASA Ames, has sufficient flexibility to specify internal and external component weights and locations. For configurations with unknown internal or external component weights and locations, the total weight is uniformly distributed over the entire volume. The outputs of interest are the mass moments of inertia and center-of-gravity location.

There are many ways to estimate or measure vehicle aerodynamics, such as semi-empirical expressions, theoretical aerodynamics, wind tunnel experimentation, computational fluid dynamics, flight experimentation, or any mixture thereof. The aerodynamic tool currently available within the IVME is the recently modified vortex-lattice code Vorview (version 1.7.1)[4], which estimates stability and control derivatives for specified operating conditions. Vorview outputs an ASCII text file and also displays a colormap image of the surface pressure distribution. A grayscale example of the colormap is shown in figure 5 for the commercial transport concept.

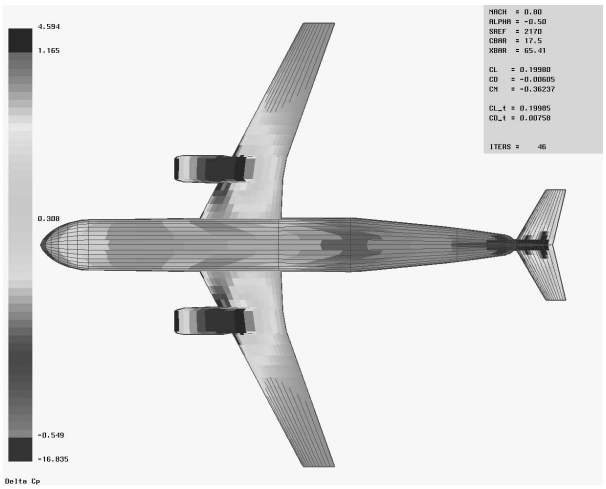

Figure 5. Grayscale Mapping of the Surface Pressure Distribution for the commercial transport model.

Vorview is executed repeatedly at a variety of operating conditions that define the flight envelope of interest. All of the ASCII text files generated by Vorview are reformatted into columns of data within one single file. The first column(s) are independent variables (typically Mach number, angle-of-attack, etc...), and the remaining columns are dependent variables, which are the stability and control derivatives.

This reformatted data is then used to train a neural network. Options available for training include a Levenberg-Marquardt (LM) multi-layer perceptron[5], and a Dynamic Cell Structure (DCS) perfect topology representation network[6], both of which can be trained to predetermined error levels. The trained network is used in the inverse model portion of the flight control architecture, described in the next section.

Simulation Environment

Once the three-dimensional RAM model of the aircraft is converted to the Open Inventor format, it can be driven by the simulation environment, which includes a generic math model, flight management system, programmable flight displays and out-the-window texture mapped terrain. The aerodynamic and inertial characteristics of each aircraft are also integrated into the math model residing in the simulation environment, a block diagram of which is shown in figure 6.

Pilot and Flight Management System Inputs

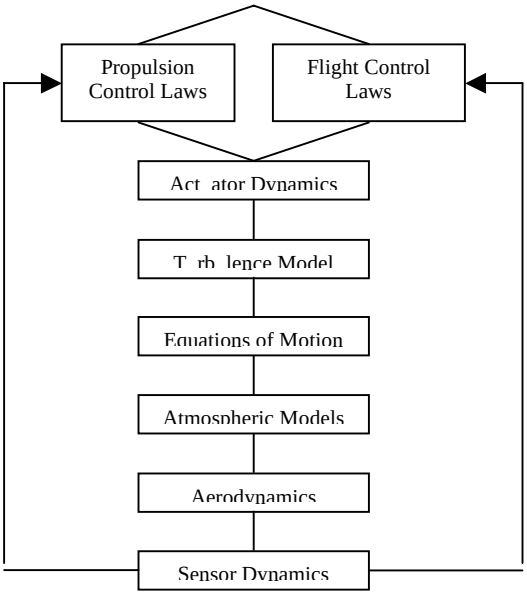

Figure 6. Math Model Residing in the Simulation Environment.

The math model that drives the graphics is complete with sensor and actuator dynamics. The equations of motion are based on perturbation theory, however most of the non-linear terms are retained in the gravitational and inertial portions of the translational axes. All of the non-linear terms are retained in the inertial portions of the rotational axes.

Environmental conditions for both Earth and Mars are modeled to account for pressure, density, temperature, gravity, and speed-of-sound variations with altitude; from mean sea level up to 282,166 feet (86 km) for Earth and 196,860 feet (60 km) for Mars. The Mars atmosphere was incorporated for an earlier study of a conceptual aircraft designed to fly on Mars.

The Earth atmosphere is based on a 1976 standard atmosphere model. The Dryden turbulence model is implemented in a separate subroutine to provide an option for simulating light, medium, or heavy turbulence levels at altitudes below 10,000 feet.

The Mars atmosphere is based on a Global Reference Atmosphere Model (GRAM), which, among other things, requires a specific reference date and trajectory.[7] The model includes crosswind variations relative to isobars (lines of constant pressure), which vary in direction and magnitude relative to altitude.

The math model is embedded in a high-fidelity workstation-based simulation architecture known as the miniACFS, shown in figure 7. The architecture is derived from the six degree-of-freedom motion-based ACFS simulator, and is complete with a full flight management system that includes both autoflight and autothrottle control.

Figure 7. miniACFS.

A texture-mapped terrain was developed for both Earth and Mars to provide high quality out-the-window visual cueing. The Earth terrain is complete with a runway, mountain ranges, and various sized hangars. The Mars terrain is modeled after Valles Marineris, which was downloaded from the internet and enhanced for incorporation into the simulation environment.

The overall dimensions for the three aircraft modeled by the IVME are given in table 1.

Table 1. Aircraft Overall Dimensions.

	Transport	F-15	UAV
Wing Area (ft^2)	2169.9	608.0	22.8
Wing Span (ft)	139.7	42.8	5.2
Length (ft)	161.3	63.8	8.3

The control surfaces enabled on the F-15 ACTIVE aircraft are ailerons (δ_a), symmetric and differential canards (δ_c, δ_{dc}), symmetric and differential stabilator (δ_s, δ_t), and rudders (δ_r). The control surfaces enabled on the commercial transport and LoFLYTE™ UAV are ailerons, elevators (δ_e), and rudder. The propulsion system is a first order lag with a 1.2 second throttle servo time constant for both manual and auto throttle control to approximate typical response characteristics. Powerplant dynamics in the form of engine gyroscopic effects can also be modeled, but were not included for the results presented in this paper.

The direct adaptive tracking controller developed by Kim and Calise and subsequently modified by NASA resides in the math model.[8,9] The control laws are based on feedback linearization theory, and are comprised of a command augmentation system (CAS) that has both an attitude orientation system and command augmentation logic. The attitude orientation system is an airframe stabilization system that accepts rate commands. This serves the function of stabilizing the airframe while following the commanded rates. The command augmentation logic is an outer loop function to track the pilot/operator commands. The

pilot/operator commands normal acceleration with longitudinal stick, roll rate with lateral stick, and yaw rate with pedals. This design provides normal acceleration and roll and yaw rate command tracking.

The output of the attitude orientation system is summed with the adaptive portion of the controller and then transformed into aircraft body axis rotational acceleration commands P_c, Q_c, and R_c. These commands are the inputs to the inverse model for calculating control surface deflections.

$$\begin{bmatrix} \delta_t \\ \delta_s \\ \delta_r \end{bmatrix} = B^{-1} \begin{bmatrix} \dot{P}_c - L_1 \\ \dot{Q}_c - M_1 \\ \dot{R}_c - N_1 \end{bmatrix} \quad (1)$$

For the F-15 ACTIVE aircraft, δ_c is scheduled with angle-of-attack and controlled independently, whereas δ_a and δ_{dc} are blended with δ_t and δ_r, respectively. The symmetric canard schedule and blending relationships are based on those used for the S/MTD conventional mode control laws.

$$\delta_a = 2\delta_t \quad (2)$$

$$\delta_{dc} = -\delta_r \quad (3)$$

For the commercial transport concept and the LoFLYTE™ UAV, δ_t and δ_s are replaced with δ_a and δ_e, respectively, in equation (1), $\delta_t = \delta_c = \delta_{dc} = 0$, and the B^{-1} matrix is revised accordingly.

A modification was made in the plant dynamics portion of the inverse model, L_1, M_1, and N_1. The original expression for these terms reflects the known plant dynamics multiplied by the aircraft states, Ax. The modification replaces Ax by simply subtracting estimated accelerations due to the controls from the body axis rotational accelerations, $\dot{x} - Bu$. The benefit of this modified approach is that only neural network estimates of the control derivatives are required in the inverse model, as opposed to both stability and control derivatives.

$$L_1 = \dot{P} - \frac{\bar{q}Sb}{I_x I_z - I_{xz}^2} \left\{ I_z \left[\begin{matrix} \overline{C}_{l_{\delta_a}} \delta_a + \overline{C}_{l_{\delta_t}} \delta_t + \\ \overline{C}_{l_{\delta_{dc}}} \delta_{dc} + \overline{C}_{l_{\delta_r}} \delta_r \end{matrix} \right] + I_{xz} \left[\begin{matrix} \overline{C}_{n_{\delta_a}} \delta_a + \overline{C}_{n_{\delta_t}} \delta_t + \\ \overline{C}_{n_{\delta_{dc}}} \delta_{dc} + \overline{C}_{n_{\delta_r}} \delta_r \end{matrix} \right] \right\} \quad (4)$$

$$M_1 = \dot{Q} - \frac{\bar{q}S\bar{c}}{I_y} \left[\overline{C}_{m_{\delta_s}} \delta_s \right] \quad (5)$$

$$N_1 = \dot{R} - \frac{\bar{q}Sb}{I_x I_z - I_{xz}^2} \left\{ I_{xz} \left[\begin{matrix} \overline{C}_{l_{\delta_a}} \delta_a + \overline{C}_{l_{\delta_t}} \delta_t + \\ \overline{C}_{l_{\delta_{dc}}} \delta_{dc} + \overline{C}_{l_{\delta_r}} \delta_r \end{matrix} \right] + I_x \left[\begin{matrix} \overline{C}_{n_{\delta_a}} \delta_a + \overline{C}_{n_{\delta_t}} \delta_t + \\ \overline{C}_{n_{\delta_{dc}}} \delta_{dc} + \overline{C}_{n_{\delta_r}} \delta_r \end{matrix} \right] \right\} \quad (6)$$

The control derivatives above are denoted with an overstrike, such as $\overline{C}_{l_{\delta_a}}$, to signify that they are neural network estimates.

The controller is based on feedback linearization theory, and no gain scheduling is required for the architecture. The gains are functions of $\overline{C}_{Z_\alpha}$ in the longitudinal CAS, and the control derivatives in the inverse model, and can be tuned to produce desirable natural frequency, w_n, and damping, ζ, characteristics of an equivalent, complex, linear second order system. Tuning is accomplished by varying the inner-loop and outer-loop time constants which, in turn, affect gains within the CAS. Properly specified inner-loop and outer-loop time constants result in defining the vehicle class, flight phase category, and level of flying qualities for a given aircraft. The controller has an option for automatic turn coordination, but it was not used for the results presented in the next section.

Results

The results presented in this section provide a basis with which to examine the capability of both the IVME and the simulation environment to model and simulate three completely different aircraft. These results are primarily influenced by the ability of RAM, Vorview, and Balance to accurately estimate the physical and aerodynamic characteristics of interest. They are also dependent on the ability of the controller to produce acceptable closed-loop dynamic characteristics of the aircraft with minimal redesign or gain scheduling.

Overall, much attention was spent in developing the RAM models of the three aircraft. Known physical

and aerodynamic characteristics were used to validate the results produced by Balance and Vorview. The LM neural network was trained on the reformatted Vorview estimates, and then used along with the Balance estimates in the inverse model portion of the controller.

The results presented in Table 2 illustrate the accuracy of Balance in estimating center-of-gravity location and inertia values, all of which are acceptable relative to actual values for that aircraft.

Table 2. IVME Modeling Accuracy of Aircraft Inertial Characteristics (%error)*.

	Transport	F-15	UAV
I_x	-3.4%	-2.9%	-20.8%
I_y	9.3%	1.1%	8.75%
I_z	6.3%	-3.2%	-8.4%
I_{xz}	-148.2%	-27.9%	83.3%
X_{CG}	-7.3%	0.3%	-10.6%
Z_{CG}	100%	-30.9%	-100%

$$^{*}\%error = \frac{(Estimated - Actual)}{Actual} x100$$

Values of I_{xz} and Z_{CG} are relatively small. The magnitude of the differences in estimated versus actual values of I_{xz} and Z_{CG} are not that great, and are on the order of the magnitude of the differences for I_z and X_{CG}, respectively. The percent errors for those parameters are large because their actual values are relatively small to begin with.

The results presented in Table 3 illustrate the accuracy of Vorview in estimating relatively important stability derivatives.[10] The speed ranges selected for each aircraft correspond to their operational envelope at sea level, with the exception of the F-15 ACTIVE aircraft. Results are not shown in the transonic region for that aircraft because they degrade significantly at those higher speeds, a known limitation of vortex-lattice methods in general.

Derivative estimates were only generated for the trim condition at each airspeed. The results are very good for nearly all of the derivatives considered. Over half of the estimates are below 10% error, and all but two derivative estimates are below 15% error. Estimates of C_{Z_α} are consistently below actual values for the F-15 ACTIVE aircraft by approximately 20%, and estimates of C_{l_β} are well below actual values for the LoFLYTE™ UAV by approximately 96%. A contributing factor to these inaccuracies may well be the differences noted between estimated and actual center-of-gravity locations. Overall, cumulative estimates are two to three times better than previous results obtained using an earlier version of Vorview.

Table 3. IVME Modeling Accuracy of Aircraft Aerodynamic Characteristics (%error)*.

M	C_{Z_α}	C_{m_α}	C_{m_q}	C_{n_β}	C_{l_β}	C_{l_p}
Tran	(%)	(%)	(%)	(%)	(%)	(%)
0.3	2.2	-14.0	-12.8	-13.1	11.8	-19.3
0.4	4.0	-7.4	-9.9	-13.9	-3.1	-12.8
0.5	2.1	11.8	-4.3	-14	-9.8	-2.6
|Avg|	**2.8**	**11.1**	**9.0**	**13.7**	**8.3**	**11.6**
F-15	(%)	(%)	(%)	(%)	(%)	(%)
0.4	-19.6	2.0	-4.2	-18.4	14.5	-1.0
0.5	-20.2	2.5	-1.7	-17.0	13.0	4.9
0.6	-20.7	-7.2	1.5	-10.3	12.8	11.5
0.7	-21.0	-3.0	6.5	-10.9	9.8	18.8
0.8	-21.2	3.0	13.6	-4.3	12.9	34.8
|Avg|	**20.5**	**3.5**	**5.5**	**12.2**	**12.6**	**14.2**
UAV	(%)	(%)	(%)	(%)	(%)	(%)
0.1	1.4	-3.9	-3.1	8.3	-96.1	-1.4
0.2	1.6	-2.8	-2.3	8.7	-96.1	-1.3
0.3	2.1	-0.8	-1.1	9.2	-96.1	-1.0
0.4	2.8	2.1	0.8	9.9	-96.1	-0.6
|Avg|	**2.0**	**2.4**	**1.8**	**9.0**	**96.1**	**1.1**

$$^{*}\%error = \frac{(Estimated - Actual)}{Actual} x100$$

It should also be noted that the utility of Vorview is realized in terms of ease-of-use, computational efficiency, and the ability to estimate rate derivatives in the absence of more reliable data generated from other experimental or computational sources.

Simulation validation for each aircraft was performed by comparing time histories of aircraft states in a maneuver. Each aircraft performed the same closed-loop maneuver with both actual data and estimates obtained using the IVME. The maneuver begins at a steady, level 1.0g condition. A roll rate step command of 10 deg/sec is given until an 80 deg bank angle is obtained. This is followed by a normal acceleration step command (3.0g for the commercial transport and 5.0g for the F-15 ACTIVE aircraft and LoFLYTE™ UAV) that is maintained until the end of the maneuver. Full throttle is held for the entire 30 second maneuver.

Figure 8 shows the roll rate and normal acceleration responses and speed profile for the commercial transport in the maneuver. The closed-loop responses generated using estimated aircraft characteristics correlate well with actual aircraft responses. Slight differences appear at the completion of the roll rate step command, on the order of 1.0

deg/sec, lasting approximately 1.0 sec. The initial and final airspeeds for the maneuver are $M_o = 0.3, M_f = 0.5$.

Although desired aircraft response is achieved, there are differences between estimated and actual aileron deflection. Aileron position is significantly under predicted. This is because estimates of $C_{l_{\delta_a}}$ are larger than actual values for the aircraft. The estimated elevator position compares well with the actual position throughout the maneuver, except for the elevator spike that occurs when normal acceleration is initially commanded to 3.0g. Finally, the rudder position is over predicted, saturating at the onset of the roll rate command, and remaining saturated throughout the maneuver. Although estimates of $C_{n_{\delta_r}}$ are accurate, estimates of C_{n_β} are 14% smaller than actual values, resulting in a requirement for a larger yaw moment provided by increased rudder deflection.

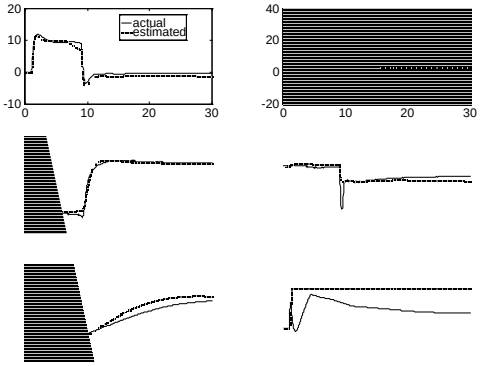

Figure 8. Commercial Transport Predicted Maneuver Response.

Figure 9 shows results for the F-15 ACTIVE aircraft in the maneuver. Again, the closed-loop responses generated using estimated aircraft characteristics correlate well with actual aircraft responses. Slight differences appear at the onset and completion of the roll rate step command, on the order of 1.0 deg/sec, lasting approximately 1.0 sec. The initial and final airspeeds for the maneuver are $M_o = 0.4, M_f = 0.9$. The final airspeed is outside of the neural network training data set boundary of $M = 0.8$.

Although desired aircraft response is achieved, significant differences are noted between estimated and actual aileron and rudder deflection. Those control surface positions are under predicted, and the differences tend to propagate while the aircraft is banking, reaching a maximum difference of 10 degrees for the ailerons and 5 degrees for the rudder before slowly converging over the remaining portion of the maneuver. This is because estimates of $C_{l_{\delta_a}}$ and $C_{n_{\delta_r}}$ are larger than actual values for the aircraft. The estimated symmetric stabilator position compares well with the actual position during the first part of the maneuver, however differences appear when normal acceleration is commanded to 5.0g. Those differences propagate to a maximum difference of 4 degrees at the end of the maneuver. Although estimates of $C_{m_{\delta_s}}$ are accurate well within the subsonic region, they become less accurate as speed increases into the transonic region.

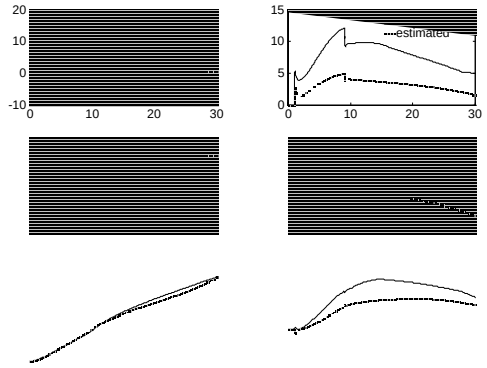

Figure 9. F-15 ACTIVE Predicted Maneuver Response.

Figure 10 shows results for the LoFLYTE™ UAV in the maneuver. The closed-loop responses generated using estimated aircraft characteristics correlate well with actual aircraft responses in the long period. Differences appear in the short period at the completion of the roll rate step command. The response generated using the IVME estimated aircraft characteristics show a 1.0 deg/sec roll rate overshoot, as opposed to a 10.0 deg/sec overshoot. This is a result of the significant difference noted between actual and estimated values of C_{l_β}. The initial and final airspeeds for the maneuver are $M_o = 0.1, M_f = 0.35$, and differences in speed begin to appear beyond $M = 0.2$.

Although desired aircraft response is achieved, significant differences are noted similar to those described for the F-15 ACTIVE aircraft, and primarily for the same reasons. Aileron and rudder positions are under predicted, and the differences tend to propagate to approximately 12 degrees before converging near the end of the maneuver. The estimated elevator position compares well with the actual deflection during the first part of the maneuver, however differences appear after normal acceleration is commanded to 5.0g. Those differences propagate to a maximum difference of 3 degrees at the end of the maneuver. As was the case with the F-15 ACTIVE aircraft, the reason for the

differences is because of inaccuracies in the control derivative estimates.

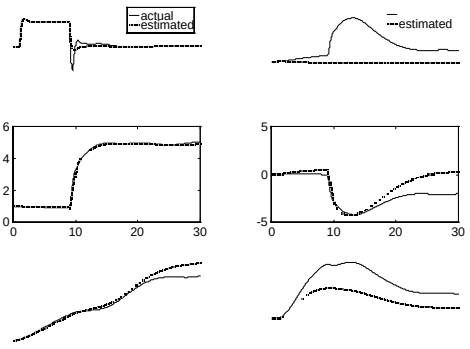

Figure 10. LoFLYTE™ Predicted Maneuver Response.

Conclusion

The results presented in the previous section demonstrate a new capability to model and simulate aircraft in different vehicle classes. An Integrated Vehicle Modeling Environment was developed and used to estimate geometric, inertial, and aerodynamic characteristics for a commercial transport concept, a modified fighter, and a small UAV. Estimated aircraft characteristics were integrated into a math model embedded in a high-fidelity simulation environment. A pre-existing flight control system residing in the math model that does not require gain scheduling or redesign was used to control each aircraft in a maneuver.

In general, the results correlate well with respect to inertial, aerodynamic, and closed-loop characteristics of each aircraft throughout a significant range of speeds. Aerodynamic derivative estimates were two to three times better than previous results obtained using an earlier version of Vorview, and closed-loop response characteristics for each aircraft were well predicted in the long period.

There were differences noted between estimated and actual control surface deflections for all three aircraft during the maneuver. This does not present a problem when operating within the authority of the control surfaces. However it is recognized that control saturation may not be well predicted under more aggressive maneuvers, as was seen with the commercial transport.

The results of a study conducted in 1987 suggest that even the most careful wind tunnel measurements of airfoil section lift-curve slope are only accurate to within +/-3.5% of their presumed actual values.[11] Interestingly, a 1995 study noted that differences begin to appear in aircraft perturbed state time histories when important stability and control derivative estimates are inaccurate beyond +/-3.77% of their known values.[12] Based on this information, it is likely that estimated and actual control surface positions would more closely match when derivative estimates are within +/-3.5%, or so. The fact that the long period response characteristics are well predicted indicates the controller is robust, essentially masking larger errors.

The results presented in this paper provide the necessary basis with which to assess the validity of the IVME to model and simulate entirely new aircraft concepts, and together with the Simulation Environment, to explore next generation intelligent flight control concepts and vehicle interface technologies. This represents the completion of a critical step toward meeting the stated goals for developing this modeling environment, and provides a value-added capability to the conceptual design and aircraft synthesis process.

References

[1] Totah, J., “Simulating Conceptual and Developmental Aircraft”, AIAA Paper 98-4161, 1998.

[2] Zeh, J. M., Young, D. L., and Couture, N. J., “STOL and Maneuver Technology Demonstrator (S/MTD) Stability Derivatives”, WL-TR-92-3055, 1992.

[3] Blake, M. W., “The NASA Advanced Concepts Flight Simulator: A Unique Transport Aircraft Research Environment”, AIAA Paper 96-3518, 1996.

[4] Miranda, L. R., Elliot, R. D., and Baker, W. M., “A Generalized Vortex Lattice Method for Subsonic and Supersonic Flow Applications”, NASA CR 2865, December, 1977.

[5] Norgaard, M., Jorgensen, C., and Ross, J., "Neural Network Prediction of New Aircraft Design Coefficients", NASA TM 112197, May 1997.

[6] Jorgensen, C. C., "Direct Adaptive Aircraft Control Using Neural Networks", NASA TM 112198, May, 1997.

[7] Justus, C. G., Johnson, D. L., and James, B. F. “A Revised Thermosphere for the Mars Global Reference Atmospheric Model (Mars-GRAM Version 3.4)”, NASA TM 10851, July 1996.

[8] Kim, B. S. and Calise, A. J., “Nonlinear Flight Control Using Neural Networks”, AIAA Journal of Guidance, Navigation, and Control, Vol. 20, No. 1, 1997.

[9] Totah, J., "Adaptive Flight Control and On-Line Learning", AIAA Paper 97-3537, 1997.

[10] Roskam, J., Airplane Flight Dynamics and Automatic Flight Controls, Part I, Roskam Aviation and Engineering Corporation, Ottawa, Kansas, 1979.

[11] McCroskey, W. J., "A Critical Assessment of Wind Tunnel Results for the NASA 0012 Airfoil", NASA TM 100019.

[12] Totah, J., "An Examination of Aircraft Aerodynamic Estimation Using Neural Networks", SAE Paper 952036, 1995.